How to cite: *Angew. Chem. Int. Ed.* **2021**, *60*, 22051 – 22056
International Edition: doi.org/10.1002/anie.202109310
German Edition: doi.org/10.1002/ange.202109310

Polycyclic Aromatic Hydrocarbons

Chiral Distorted Hexa-*peri*-hexabenzocoronenes Bearing a Nonagon-Embedded Carbohelicene

Miguel A. Medel, Carlos M. Cruz, Delia Miguel, Victor Blanco, Sara P. Morcillo, and Araceli G. Campaña**

Abstract: *A new family of chiral saddle-helix hybrid nanographenes is reported. The first hexa-peri-hexabenzocoronene (HBC) analogues bearing a nine-membered carbocycle are presented. Furthermore, for the first time, π-extended carbo[n]helicenes containing a nine-membered ring as part of the helical moiety have been synthesized. The combination of a [5]helicene moiety and a nonagon ring in a single chiral motif induces a tremendous distortion from planarity into the nanographenic structures compared to other saddle-helix hybrids such as heptagon- and octagon-containing π-extended carbo[5]helicenes. In fact, the interplanar angle of the two terminal rings reaches the largest angle (134.8°) of a carbohelicene reported to date, thus being by far the most twisted helicene yet prepared. Photophysical properties evaluation showed improved absorption dissymmetry factors ($|g_{abs}|= 4.2\times10^{-3}$) in the new family of nonagon-containing π-extended carbo[5]helicenes.*

Introduction

Chiral non-planar nanographenes have attracted the attention of chemists, physicists and material scientists in recent years.[1] The unique electronic, optical and dynamic properties of these systems along with their high solubility and processability, compared with their planar counterparts,[2] make them of great interest in nanoscience.[3] Undoubtedly one of the greatest attractions is the inherent chirality arising from their three-dimensional structure. However, the success of non-planar nanographenes as chiral materials in organic electronics[4] depends on attaining stereochemically rigid structures with high configurational stability, thus enabling their homochiral isolation.[5] For this reason, the study of chiroptical properties in novel enantiopure distorted π-systems is a growing topic nowadays,[6] which shifted from simple academic curiosity to become an important research field. To date, these studies allowed to furnish molecular materials with potential to be used in a wide variety of applications in the field of organic electronics,[7] such as spin filters, chiroptical switches or sensors.[8] As a result, considerable efforts are currently ongoing to synthesize such chiral polycyclic aromatic hydrocarbons (PAHs). Typical strategies include the combination of multiple carbo[*n*]helicenes in a single structure,[9] the introduction of helical moieties within planar π-extended PAHs[10] such as hexa-*peri*-hexabenzocoronenes (HBCs) (also known as "superhelicenes" or "supertwistacenes") or the combination of non-planar PAHs and carbo[*n*]helicenes in the same structure.[11] The latter strategy enables the study of chiroptical properties raised from novel twisted and curved aromatic surfaces in a single π-system.[12]

Very recently, our group has developed an unprecedented strategy for the insertion of saddle curvature into both the carbohelicene and the HBC unit, leading to rigid chiral helical nanographenes.[13] Typically, the replacement of one or more six-membered rings by four-, five- or seven-membered rings

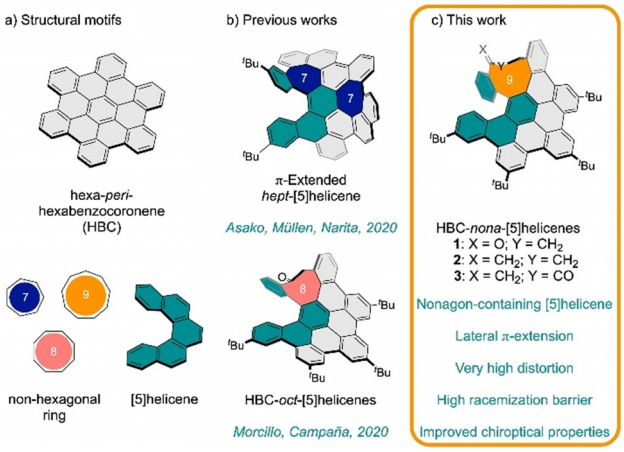

Figure 1. a) Common structural motifs present in π-extended carbo-[5]helicenes containing non-hexagonal rings; b) Previously reported HBC analogues *hept*-[5]helicene and HBC-*oct*-[5]helicene; c) General structure of the new family of HBC-*nona*-[5]helicene and their main properties.

[*] M. A. Medel, Dr. V. Blanco, Dr. S. P. Morcillo, Dr. A. G. Campaña
Departamento de Química Orgánica, Unidad de Excelencia de Química (UEQ), Facultad de Ciencias, Universidad de Granada
18071 Granada (Spain)
E-mail: samorcillo@ugr.es
araceligc@ugr.es
Dr. C. M. Cruz
Department of Chemistry, Faculty of Science, University of Zurich
Winterthurerstrasse 190, 8057 Zurich (Switzerland)
Dr. D. Miguel
Departamento de Fisicoquímica, Facultad de Farmacia, UEQ, Universidad de Granada
18071 Granada (Spain)
Supporting information and the ORCID identification number(s) for the author(s) of this article can be found under: https://doi.org/10.1002/anie.202109310.

in a carbo[*n*]helicene leads to a significant decrease of the configurational stability.[14] However, Müllen and Narita proved that the simultaneous inclusion of two heptagonal carbocycles into both the π-extended structure and the carbo[5]helicene (Figure 1) gives rise to more rigid structures ($\Delta G^{\ddagger} = 25.41$ kcal mol^{-1} at 298 K)[15] than either carbo-[5]helicenes or nanographenes containing heptagonal rings alone. For its part, the group of Ravat has recently shown that the inclusion of a heptagonal ring fused to pyrene motifs also increases the enantiomerization barrier compared to its fully hexagonal [5]helicene counterpart.[16] In this line, we have demonstrated that a HBC bearing an octagon-containing carbo[5]helicene, namely HBC-*oct*-[5]helicene (Figure 1), exhibits the largest torsion angle ($\theta = 79.5°$) reported so far for a carbo[5]helicene.[13] The above strategy allowed us to design much more rigid structures ($\Delta G^{\ddagger} > 38.3$ kcal mol^{-1} at 473 K) than distorted nanographenes containing either octagonal rings or simple carbo[5]helicenes. At this point, we wondered if we could go a step further by introducing a nonagonal carbocycle into the π-extended carbo[5]helicene. This concept would allow us to study whether the introduction of a larger carbocycle leads to more rigid chiral motifs with improved chiroptical properties, affording an insight into the limits of distortion and the stability in saddle-helix hybrid nanographenes.

The inclusion of larger, $n > 8$, membered rings into a carbohelicene and/or π-extended systems is an unexplored area where higher-order derivatives ($n = 9$) have exclusively been studied in two diazatrioxa[9]-circulene derivatives.[17] To the best of our knowledge, neither saddle-shaped nonagon-containing HBCs nor nonagon-containing carbohelicene as chiral motif have been reported before.

Herein, we report the first examples of doubly distorted HBCs bearing a nonagon-containing carbohelicene, called as HBC-*nona*-[5]helicene. The effect of the distortion on the structural stability and rigidity, and on the chiroptical properties of these highly distorted nanographene-like structures is exhaustively studied and discussed.

Results and Discussion

The synthetic route towards HBC-*nona*-[5]helicenes **1**–**3** is depicted in Scheme 1. The starting point was the synthesis of the HBC-*oct*-[5]helicene **5** following our previous methodology.[13] Herein, the key step relies on a single ring expansion (70%) from the eight-membered ring **5** to the nine-membered ring **1**, where the rest of the structure is kept unaltered. The incorporation of the ketone moiety allows an easy derivatization of the structure. Thus, to create a small family of nonagon-containing HBCs, we envisioned two new derivatives, all-carbon analog **2**, and derivative **3** which could lead to different distortions in the HBC core. The reactivity of the ketone moiety allowed us the synthesis of **2** (57%), and the subsequently allylic oxidation using selenium-dioxide led to compound **3** (75%).

Similar to the family of HBC-*oct*-[5]helicenes, the new family of HBC-*nona*-[5]helicenes is very soluble in common organic solvents, thus allowing their full characterization by

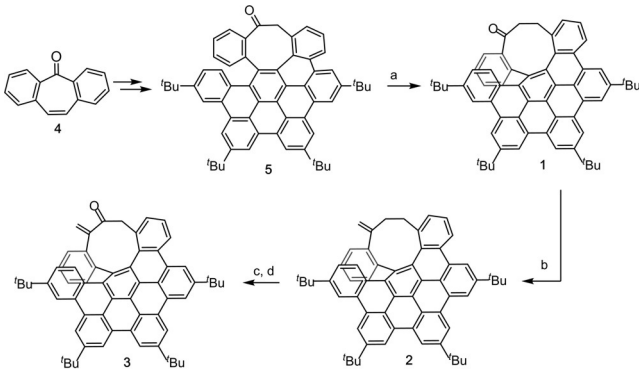

Scheme 1. Synthesis of **1**–**3**. Reagents and conditions: a) i) $BF_3{\cdot}OEt_2$, $TMSCHN_2$, CH_2Cl_2, 0 °C, 5 min; ii) $Bu_4NF{\cdot}3H_2O$, THF, 1 h, 70%; b) Tebbe's reagent, THF, 0 °C 5 min, 57%; c) SeO_2, dioxane, 100 °C, 1 h; d) DMP, CH_2Cl_2, 0 °C to rt, 4 h, 75%.

^{1}H, ^{13}C and 2D NMR spectroscopy as well as HRMS (see SI, Figures S22–S31 and S32–34, respectively). The structure of compound **3** was further confirmed by single-crystal X-ray diffraction (Figure 2). Single crystals were grown by vapor diffusion of acetonitrile into a chloroform solution of **3**.

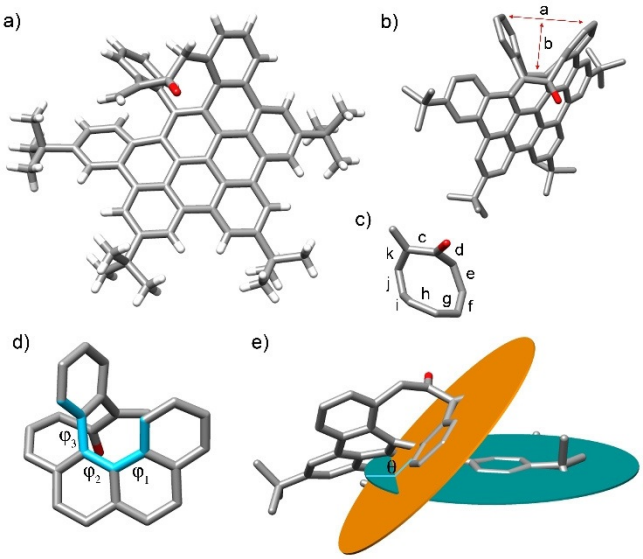

Figure 2. a) X-ray structure of compound **3**; b) Dimensions of the saddle induced by the nonagon being embedded in the [5]helicene moiety. Distances [Å]: a: 4.90–5.10 b: 3.08–3.14; (see supporting information); c) Detail of the structure of the nine-membered ring. C–C distances [Å]: c, 1.50; d, 1.52–1.53; e, 1.53; f, 1.42; g, 1.47–1.48,h, 1.41; i, 1.50; j, 1.40; k, 1.48; d) Detail of the three dihedral angles in the rim ($\varphi_1 = 26.5$–$27.1°$; $\varphi_2 = 2.4$–$2.5°$; $\varphi_3 = 106.9$–$108.3°$). The average of the three dihedral angles leads to the average torsion angle of $\varphi = 45.2$–$46.0°$; e) Interplanar angle ($\theta = 134.8°$) of the mean planes (in green and orange) of the two terminal benzene rings. H atoms (in b–e) and solvent molecules have omitted for clarity. Color code: C (gray), H (white), O (red). A range is given for some distances and angles as two molecules of **3** are found in the unit cell. Deposition Number 2096027 contains the supplementary crystallographic data for this paper. These data are provided free of charge by the joint Cambridge Crystallographic Data Centre and Fachinformationszentrum Karlsruhe Access Structures service www.ccdc.cam.ac.uk/structures.

Crystallographic analysis of **3** confirmed the expected helical structure and revealed that the inclusion of a nonagonal ring into both the helicene and the HBC unit leads to the most distorted carbo[5]helicene synthetized to date (Figure 2). It was found that the interplanar angle of the two terminal rings is completely twisted giving rise to an exceptional value of 134.8° (θ, see Figure 2e). This value is almost three times higher than the one found in pristine carbo[5]helicene (46°)[18] or twice the multiple hexapole-[5]helicene (69°).[9c–d] In fact, comparing with hept-[5]helicene (77.3°)[15] or even HBC-*oct*-[5]helicene (80.8°),[13] the terminal ring of **3** is completely twisted, phenomenon that has been described for twistacenes but with no precedent in helicenes.[19] The helicity and distortion of the helicenes and PAHs mostly are determined in terms not only of the interplanar angle between the mean planes of the terminal benzene rings (θ), related to the degree of compression of helical molecules, but also in terms of the torsion angles (φ), which represents the degree of the twist of a helix (Figure 2d,e). Both terms also depend on the number and type of rings that make up the helicene skeleton. In this sense, we demonstrate that the inclusion of nonagon ring has a tremendous effect on the average torsion-angle since it is also much bigger (45.2–46.0°) than those previously reported: *hept*-[5]helicene (35.6°),[15] HBC-*oct*-[5]helicene (35.0°),[13] carbo-[5]helicene (22.1°)[18] or the multiple hexapole[5]helicene (22.1–22.2°).[9c–d] In fact, the large ring ($n=9$) is responsible for the maximal dihedral angle in the rim ($\varphi_3=106.9°–108.3°$, see Figure 2d). To the best of our knowledge, this value represents the highest dihedral angle reported in a helicene and, therefore, being the HBC-*nona*-[5]-helicene the most highly twisted helicene yet prepared. Unlike reported diazatrioxa[9]circulenes,[17] in which the nonagon is mainly flat with a slight distortion from planarity, in compound **3** the nine-membered ring displays a deep saddle-shape with a distorted boat-boat geometry.[20] The inclusion of the nonagon in the upper part of the HBC leads to a saddle-shape backbone of 3.08–3.14 Å deep and 4.90–5.10 Å wide. The nonagon is irregular as the C–C distances of those bonds non-fused with the benzene rings (c–e, i, k in Figure 2c) are larger (1.48–1.53 Å) than those of the bonds fused with benzene rings (1.40–1.42 Å) (f–h, j in Figure 2c), except for one of the latter, which displays a distance of 1.47–1.48 Å (g in Figure 2c). Remarkable, we obtained good agreement between theoretical and crystal structures of **3**. Although we could not obtain single crystals of **1** and **2**, optimized theoretical structures **1–3** showed similar deep distortion in all compounds, with the highest twisted angle between helicene terminal rings for the case of **3** (see SI, Figures S37-39).

The electronic effect of embedding a nonagon-ring moiety into a π-extended carbo[5]helicene was studied by optical spectroscopy. The absorption and emission spectra of **1–3** in various polar and nonpolar solvents were covered. Dichloromethane (DCM) solutions of **1–3** displayed a broad absorption band centered at 351 nm ($\varepsilon=8.8\times10^4\ M^{-1}cm^{-1}$), 352 nm ($\varepsilon=1.1\times10^5\ M^{-1}cm^{-1}$) and 355 nm ($\varepsilon=8.0\times10^4\ M^{-1}cm^{-1}$), respectively (see Figure 3). All three compounds showed a significant bathochromic shift in their absorption spectra

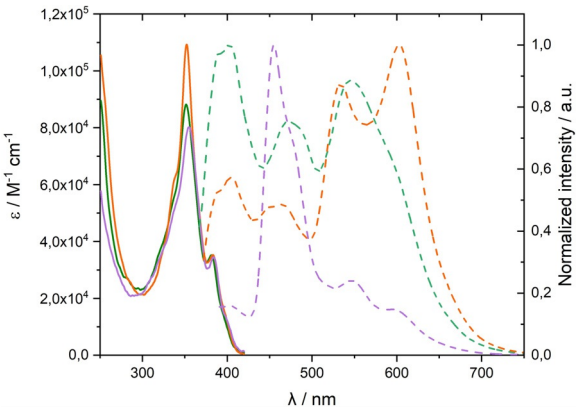

Figure 3. UV/Vis (solid lines) and normalized fluorescence ($\lambda_{exc}=350$ nm, dashed lines) spectra of **1** (green), **2** (orange) and **3** (purple) in DCM.

compared to parent [5]helicene ($\lambda_{max}=289$ nm) and, as expected, they were in the same range as those reported for *hexakis-tert*-butyl-HBC (*t*Bu-HBC, $\lambda_{max}=359$ nm)[10a] or the family of HBC-*oct*-[5]helicenes[13] ($\lambda_{max}=342–356$ nm). Furthermore, the absorption onset of compounds **1**, **2** and **3** (410 nm, 412 nm and 413 nm) provided an optical band gap of 3.02 eV, 3.01 eV and 3.00 eV, respectively. These values are slightly higher than those found for HBC-*oct*-[5]helicenes[13] or *t*Bu-HBC[10a] and lower than the ones reported for [5]helicene.[21] In addition, we studied the electrochemical behavior of **1–3** by cyclic voltammetry in CH_2Cl_2 (ca. 1.5×10^{-3} M), finding one reversible oxidation wave for compounds **1–3**, with a half-wave oxidation potential of 0.83 V, 0.77 V and 0.78 V (vs. Fc/Fc^+, see SI, Figures S19–S21), respectively. From these half-wave oxidation potentials, the HOMO energy levels of **1–3** were evaluated as −5.93 eV, −5.87 eV and −5.88 eV, respectively.[22] The experimental results were well supported by DFT calculations (CAM-B3LYP/6-31G(d,p)), which estimated a similar progression in the energies of the HOMO orbitals of **1–3**, with values of −6.35 eV, −6.25 eV and −6.28 eV, respectively.

Solutions of **1–3** in DCM exhibited blue to red fluorescence when excited at 350 nm (maximum λ_{em}, apparent quantum yield (Φ_F): **1** (404 nm, 5%), **2** (604 nm, 18%) and **3** (456 nm, 11%). It is worth noting that the family of HBC-*nona*-[5]helicene presented higher Φ_F values than the pristine [5]-helicene (4%) or *t*Bu-HBC (3%)[10a] and, overall, the previous reported HBC-*oct*-[5]helicenes (2–13%). Surprisingly, quite rich fluorescence profiles are displayed for three derivatives, with four bands present in quite different proportions depending on the compound. Thus, all carbon compound **2** presents a clear maximum at around 460 nm whereas a large red-shift was obtained for α,β-unsaturated ketone **3** (λ_{em} centered at 600 nm). Fluorescence emission of **1–3** showed several fluorescence lifetimes in DCM indicative of the presence of several species in the excited state, with average fluorescence lifetimes in the maximum of emission of 6.5, 8.3 and 10.9 ns, respectively (see Tables S1–S3 in the SI). To shed light into the observed emission profiles, a more detail study of the radiative emission of HBC-nona-[5]helicene family **1–3** was developed, revealing a non-trivial

deactivation of the excited states. Firstly, we observed an excitation-dependent emission for all compounds, both in terms of intensity and also fluorescence profile (see SI, Figures S7–S9). Secondly, we studied the solvatochromism of these compounds performing fluorescence measurements in apolar (hexane) and polar protic (CH_3OH) and aprotic (CH_3CN) solvents, observing that both the shape and intensity of the bands were strongly dependent of the solvent (see Figures S10-S12). Thus, the fluorescence of **1** and **3** was strongly quenched by CH_3OH (lowering the Φ_F from 5 to 10 times, respectively), which is in a good agreement with their structure, as the presence of a carbonyl group twisted out of the molecular plane can be the responsible of such effect.[23] On the other hand, the highest decrease for all-carbon **2** was observed in hexane. In this sense, it was also found that the Φ_F values in different solvents range from 0.6% to 10% for **1**, 4.3% to 17.7% for **2** and 1.1% to 10.9% for **3**. This phenomenon was also observed in the average fluorescence lifetime values (τ), ranging from 4.1 to 12.8 ns in **1**, 6.6 to 12.6 ns in **2** and 9.0 to 13.7 ns in **3** (for more details see SI, Tables S1–S3). Finally, kinetic measurements revealed that fluorescence profiles significantly changed upon irradiation time.[24]

Chiral resolution of **1**–**3** was achieved by chiral stationary phase HPLC (CSP-HPLC) (for details see the SI). The enantiopure compounds demonstrated excellent configurational stability and tolerance against racemization due to the incorporation of a nonagon ring into the carbo[5]helicene as a rigid chiral motif. In this sense, we found that neither racemization nor decomposition were observed after heating *n*-heptane solutions of each enantiopure compound **1**–**3** at 90 °C for 6 h, as observed by variable temperature electronic circular dichroism (VT-ECD) kinetic measurements, providing a lower limit to the barrier of racemization of $\Delta G^{\neq} > 28.9\ kcal\,mol^{-1}$ at 363 K (see SI for more details).

After racemic resolution, the chiroptical properties were studied. The ECD spectra of the isolated enantiomers of **1**–**3** in DCM were recorded. Both enantiomers of each compound displayed mirror images with several opposite Cotton effect in the UV/Vis region (Figure 4). For **1**, the first eluted CSP-HPLC fraction showed two bands of major intensity with opposite Cotton effect. The first one showed a positive Cotton effect at 281 nm ($|\Delta\varepsilon| = 90.3\ M^{-1}cm^{-1}$, $|g_{abs}| = |\Delta\varepsilon|/\varepsilon = 4.1 \times 10^{-3}$) while the second one showed a negative Cotton effect at 350 nm ($|\Delta\varepsilon| = 51.5\ M^{-1}cm^{-1}$, $|g_{abs}| = 5.8 \times 10^{-4}$, Figure 4, top). Similarly, the first eluted peak after CSP-HPLC separation of **2** also exhibited two bands of major intensity, with the same Cotton effects than **1**, at 284 nm ($|\Delta\varepsilon| = 113.3\ M^{-1}cm^{-1}$, $|g_{abs}| = 4.2 \times 10^{-3}$) and 348 nm ($|\Delta\varepsilon| = 81.4\ M^{-1}cm^{-1}$, $|g_{abs}| = 7.4 \times 10^{-4}$, Figure 4, middle). However, **3** showed a more complex ECD spectrum than the previous compounds, and similarly, the first eluted peak showed the most intense positive band at 281 nm ($|\Delta\varepsilon| = 110.0\ M^{-1}cm^{-1}$, $|g_{abs}| = 3.9 \times 10^{-3}$). To sum up, the major $|\Delta\varepsilon|$ and $|g_{abs}|$ values of this HBC-*nona*-[5]helicene backbone ranged 90–113 $M^{-1}cm^{-1}$ and 3.9–4.2 $\times 10^{-3}$, respectively, a notable more than 2× fold increase in comparison with analogous previously described HBC-*oct*-[5]helicene family (Figure 1).

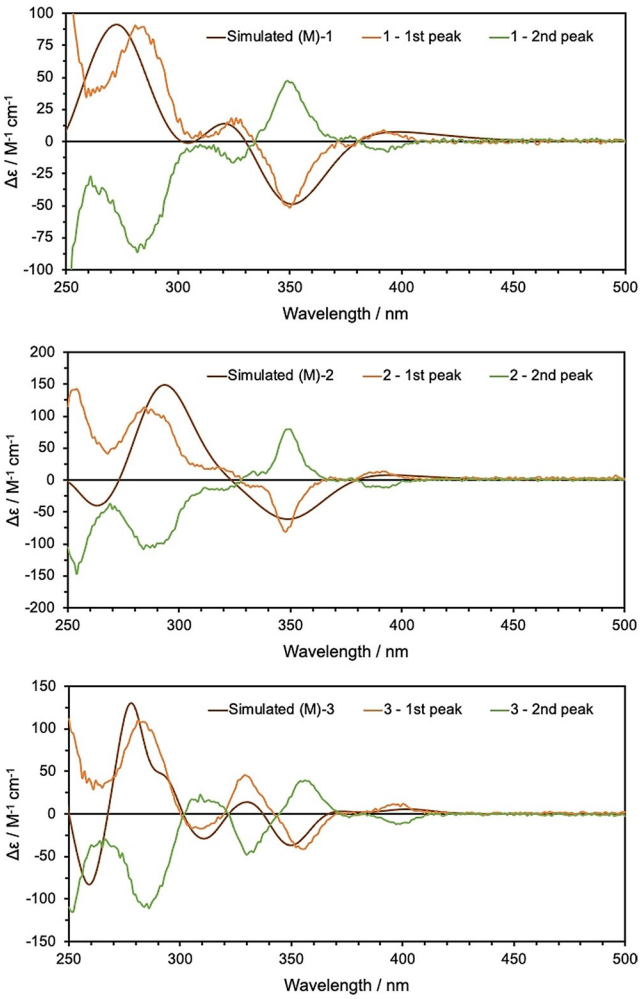

Figure 4. Top: Experimental ECD spectra of (*M*)- (orange) and (*P*)-**1** (green) in DCM (1.2×10^{-5} and 1.2×10^{-5} M, respectively) and simulated (CAM-B3LYP/6-311++G(d,p), IEFPCM DCM) ECD spectra of (*M*)-**1**. Middle: Experimental ECD spectra of (*M*)- (orange) and (*P*)-**2** (green) in DCM (1.0×10^{-5} and 1.1×10^{-5} M, respectively) and simulated (CAM-B3LYP/6-311++G(d,p), IEFPCM DCM) ECD spectra of (*M*)-**2**. Bottom: Experimental ECD spectra of (*M*)- (orange) and (*P*)-**3** (green) in DCM (1.3×10^{-5} and 1.4×10^{-5} M, respectively) and simulated (CAM-B3LYP/6-311++G(d,p), IEFPCM DCM) ECD spectra of (*M*)-**3**.

In the three compounds **1**–**3** the first CSP-HPLC eluted peaks showed a positive Cotton effect in the longest wavelength band at 392 ($|\Delta\varepsilon| = 8.9\ M^{-1}cm^{-1}$, $|g_{abs}| = 6.1 \times 10^{-4}$), 392 ($|\Delta\varepsilon| = 13.3\ M^{-1}cm^{-1}$, $|g_{abs}| = 7.3 \times 10^{-4}$) and 396 nm ($|\Delta\varepsilon| = 11.5\ M^{-1}cm^{-1}$, $|g_{abs}| = 8.9 \times 10^{-4}$, Figure 4), respectively. This band was also well predicted by TD-DFT calculations (CAM-B3LYP/6–311++G(d,p)) in all the studied HBC-*nona*-[5]helicene members and it is mainly governed by the $S_0 \rightarrow S_2$ transition (Table S4).

Notably, the calculated $|g_{abs}|$ value of the $S_0 \rightarrow S_1$ transition of HBC-*oct*-[5]helicene (Figure 1) compared to its homologous **1** with the simplest structural change (only an additional methylene unit, going from 8- to 9-membered carbocycle) is almost four times higher (see SI, Table S5). The inclusion of a larger ring in the helical moiety decreases the magnitude of the transition electric dipole moment, thus

resulting on an increment of the resulting g_{abs} value in **1**.[25] Moreover, the $S_0 \rightarrow S_1$ transition is directly related to the $S_1 \rightarrow S_0$ transition and, therefore, higher circularly polarized luminescence (CPL) responses would be expected for **1** compared to HBC-*oct*-[5]helicenes. Unfortunately, emission profiles of this HBC-*nona*-[5]helicene family are non-trivial as kinetic fluorescence measurements revealed changes in the emission profiles under the long-time irradiation required for CPL measurements preventing its recording. Nevertheless, these results show again an enhancement on the chiroptical response upon inclusion of a larger carbocycle (9- *vs.* 8-membered carbocycle) in the structure. Finally, the absolute configurations of the different enantiomers were assigned by comparing the experimental ECD spectra with TD-DFT simulated spectra for (*M*)-enantiomers of **1**–**3** (Figure 2). Therefore, the first and second eluted peaks after CSP-HPLC were assigned as (*M*)- and (*P*)-enantiomers, respectively, in all the studied compounds.

Conclusion

In conclusion, a new family of distorted chiral HBC analogues have been presented and studied. For the first time, a nine-membered carbocycle is included within the HBC backbone leading to a high distortion from planarity with a deep saddle curvature. Furthermore, being the nonagon also a constituent of a carbo[5]helicene, it gives rise to the highest distorted [5]helicene reported to date. This unprecedented chiral moiety coined as *nona-[5]helicene* induces remarkable high rigidity and stability in the saddle-helix hybrid nanographenes which exhibit high isomerization barrier and interesting chiroptical properties. Further functionalization can also be envisioned, opening the possibility of incorporating and combining those highly distorted HBCs as chiral units into larger PAHs. This strategy can lead to highly distorted saddle-helix hybrid graphenic structures exhibiting promising photophysical properties of great interest in the development of novel molecular materials.

Acknowledgements

We acknowledge the European Research Council (ERC) under the European Union's Horizon 2020 research and innovation program (ERC-2015-STG-677023), the Ministerio de Ciencia, Innovación y Universidades (MICIU/FEDER/AEI, Spain, PGC2018-101181-B-I00), the Universidad de Granada (UGR) (Plan Propio – Intensificación de la Investigación PP2017-PRI.I-02) and the Swiss National Science Foundation (Spark 2019 Grant CRSK-2_190365) for financial support. We thank the CSIRC-Alhambra, the Service and Support for Science IT (S^3IT) of the University of Zurich and Prof. Dr. Michal Juríček for supercomputing facilities. Funding for open access charge: Universidad de Granada/CBUA.

Conflict of Interest

The authors declare no conflict of interest.

Keywords: chirality · helicenes · nanographenes · nonagonal carbocycle · polycyclic aromatic hydrocarbons

[1] S. H. Pun, Q. Miao, *Acc. Chem. Res.* **2018**, *51*, 1630 – 1642.
[2] J. Wu, W. Pisula, K. Müllen, *Chem. Rev.* **2007**, *107*, 718 – 747.
[3] M. Ball, Y. Zhong, Y. Wu, C. Schenck, F. Ng, M. Steigerwald, S. Xiao, C. Nuckolls, *Acc. Chem. Res.* **2015**, *48*, 267 – 276.
[4] a) H. Isla, J. Crassous, *C. R. Chim.* **2016**, *19*, 39 – 49; b) Y. Yang, B. Rice, X. Shi, J. R. Brandt, R. Correa da Costa, G. J. Hedley, D.-M. Smilgies, J. M. Frost, I. D. W. Samuel, A. Otero-de-la-Roza, E. R. Johnson, K. E. Jelfs, J. Nelson, A. J. Campbell, M. J. Fuchter, *ACS Nano* **2017**, *11*, 8329 – 8338; c) Z. Ma, T. Winands, N. Liang, D. Meng, W. Jiang, N. L. Doltsinis, Z. Wang, *Sci. China Chem.* **2020**, *63*, 208 – 214.
[5] a) M. Rickhaus, M. Mayor, M. Juríček, *Chem. Soc. Rev.* **2016**, *45*, 1542 – 1556; b) Y. Segawa, H. Ito, K. Itami, *Nat. Rev. Mater.* **2016**, *1*, 15002; c) M. Rickhaus, M. Mayor, M. Juríček, *Chem. Soc. Rev.* **2017**, *46*, 1643 – 1660; d) M. A. Majewski, M. Stępień, *Angew. Chem. Int. Ed.* **2019**, *58*, 86 – 116; *Angew. Chem.* **2019**, *131*, 90 – 122.
[6] C. M. Cruz, S. Castro-Fernández, E. Maçôas, A. Millán, A. G. Campaña, *Synlett* **2019**, *30*, 997 – 1002.
[7] Y. Zhong, B. Kumar, S. Oh, M. T. Trinh, Y. Wu, K. Elbert, P. Li, X. Zhu, S. Xiao, F. Ng, M. L. Steigerwald, C. Nuckolls, *J. Am. Chem. Soc.* **2014**, *136*, 8122 – 8130.
[8] a) T. Verbiest, S. V. Elshocht, M. Kauranen, L. Hellemans, J. Snauwaert, C. Nuckolls, T. J. Katz, A. Persoons, *Science* **1998**, *282*, 913 – 915; b) V. Kiran, S. P. Mathew, S. R. Cohen, I. H. Delgado, J. Lacour, R. Naaman, *Adv. Mater.* **2016**, *28*, 1957 – 1962; c) R. Naaman, D. H. Waldeck, *Annu. Rev. Phys. Chem.* **2015**, *66*, 263 – 281.
[9] a) W. Yue, W. Jiang, M. Böckmann, N. L. Doltsinis, Z. Wang, *Chem. Eur. J.* **2014**, *20*, 5209 – 5213; b) X.-Y. Wang, X.-C. Wang, A. Narita, M. Wagner, X.-Y. Cao, X. Feng, K. Müllen, *J. Am. Chem. Soc.* **2016**, *138*, 12783 – 12786; c) V. Berezhnaia, M. Roy, N. Vanthuyne, M. Villa, J. V. Naubron, J. Rodriguez, Y. Coquerel, M. Gingras, *J. Am. Chem. Soc.* **2017**, *139*, 18508 – 18511; d) T. Hosokawa, Y. Takahashi, T. Matsushima, S. Watanabe, S. Kikkawa, I. Azumaya, A. Tsurusaki, K. Kamikawa, *J. Am. Chem. Soc.* **2017**, *139*, 18512 – 18521; e) M. Roy, V. Berezhnaia, M. Villa, N. Vanthuyne, M. Giorgi, J. V. Naubron, S. Poyer, V. Monnier, L. Charles, Y. Carissan, D. Hagebaum-Reignier, J. Rodriguez, M. Gingras, Y. Coquerel, *Angew. Chem. Int. Ed.* **2020**, *59*, 3264 – 3271; *Angew. Chem.* **2020**, *132*, 3290 – 3297.
[10] a) D. Reger, P. Haines, F. W. Heinemann, D. M. Guldi, N. Jux, *Angew. Chem. Int. Ed.* **2018**, *57*, 5938 – 5942; *Angew. Chem.* **2018**, *130*, 6044 – 6049; b) P. J. Evans, J. Ouyang, L. Favereau, J. Crassous, I. Fernández, J. Perles, N. Martin, *Angew. Chem. Int. Ed.* **2018**, *57*, 6774 – 6779; *Angew. Chem.* **2018**, *130*, 6890 – 6895; c) M. M. Martin, F. Hampel, N. Jux, *Chem. Eur. J.* **2020**, *26*, 10210 – 10212; d) M. Feofanov, V. Akhmetov, D. I. Sharapa, K. Amsharov, *Org. Lett.* **2020**, *22*, 5741 – 5745; e) S. Ma, J. Gu, C. Lin, Z. Luo, Y. Zhu, J. Wang, *J. Am. Chem. Soc.* **2020**, *142*, 16887 – 16893; f) Y. Chen, C. Lin, Z. Luo, Z. Yin, H. Shi, Y. Zhu, J. Wang, *Angew. Chem. Int. Ed.* **2021**, *60*, 7796 – 7801; *Angew. Chem.* **2021**, *133*, 7875 – 7880; g) Z. Qiu, C.-W. Ju, L. Frédéric, Y. Hu, D. Schollmeyer, G. Pieters, K. Müllen, A. Narita, *J. Am. Chem. Soc.* **2021**, *143*, 4661 – 4667; h) D. Reger, P. Haines, K. Y. Amsharov, J. A. Schmidt, T. Ullrich, S. Bönisch, F. Hampel, A. Görling, J. Nelson, K. E. Jelfs, D. M. Guldi, N. Jux, *Angew.*

Chem. Int. Ed. **2021**, *60*, 18073 – 18081; *Angew. Chem.* **2021**, *133*, 18221 – 18229.

[11] a) T. Fujikawa, Y. Segawa, K. Itami, *J. Org. Chem.* **2017**, *82*, 7745 – 7749; b) C. M. Cruz, I. R. Márquez, I. F. A. Mariz, V. Blanco, C. Sánchez-Sánchez, J. M. Sobrado, J. A. Martín-Gago, J. M. Cuerva, E. Maçôas, A. G. Campaña, *Chem. Sci.* **2018**, *9*, 3917 – 3924; c) C. M. Cruz, S. Castro-Fernández, E. Maçôas, J. M. Cuerva, A. G. Campaña, *Angew. Chem. Int. Ed.* **2018**, *57*, 14782 – 14786; *Angew. Chem.* **2018**, *130*, 14998 – 15002; d) C. M. Cruz, I. R. Márquez, S. Castro-Fernández, J. M. Cuerva, E. Maçôas, A. G. Campaña, *Angew. Chem. Int. Ed.* **2019**, *58*, 8068 – 8072; *Angew. Chem.* **2019**, *131*, 8152 – 8156; e) X. Yang, F. Rominger, M. Mastalerz, *Angew. Chem. Int. Ed.* **2019**, *58*, 17577 – 17582; *Angew. Chem.* **2019**, *131*, 17741 – 17746; f) J. Ma, Y. Fu, E. Dmitrieva, F. Liu, H. Komber, F. Hennersdorf, A. A. Popov, J. J. Weigand, J. Liu, X. Feng, *Angew. Chem. Int. Ed.* **2020**, *59*, 5637 – 5642; *Angew. Chem.* **2020**, *132*, 5686 – 5691; g) Y. Han, Z. Xue, G. Li, Y. Gu, Y. Ni, S. Dong, C. Chi, *Angew. Chem. Int. Ed.* **2020**, *59*, 9026 – 9031; *Angew. Chem.* **2020**, *132*, 9111 – 9116.

[12] a) I. R. Márquez, S. Castro-Fernández, A. Millán, A. G. Campaña, *Chem. Commun.* **2018**, *54*, 6705 – 6718; b) E. M. Muzammil, D. Halilovic, M. C. Stuparu, *Commun. Chem.* **2019**, *2*, 58.

[13] M. A. Medel, R. Tapia, V. Blanco, D. Miguel, S. P. Morcillo, A. G. Campaña, *Angew. Chem. Int. Ed.* **2021**, *60*, 6094 – 6100; *Angew. Chem.* **2021**, *133*, 6159 – 6165.

[14] P. Ravat, *Chem. Eur. J.* **2021**, *27*, 3957 – 3967.

[15] Z. Qiu, S. Asako, Y. Hu, C.-W. Ju, T. Liu, L. Rodin, D. Schollmeyer, J.-S. Laurent, K. Mullen, A. Narita, *J. Am. Chem. Soc.* **2020**, *142*, 14814 – 14819.

[16] A. K. Swain, K. Kolanji, C. Stapper, P. Ravat, *Org. Lett.* **2021**, *23*, 1339 – 1343.

[17] a) S. K. Pedersen, K. Eriksen, H. Ågren, B. F. Minaev, N. N. Karaush-Karmazin, O. Hammerich, G. V. Baryshnikov, M. Pittelkow, *J. Am. Chem. Soc.* **2020**, *142*, 14058 – 14063; b) S. K. Pedersen, K. Eriksen, N. N. Karaush-Karmazin, B. Minaev, H. Ågren, G. V. Baryshnikov, M. Pittelkow, *Angew. Chem. Int. Ed.* **2020**, *59*, 5144 – 5150; *Angew. Chem.* **2020**, *132*, 5182 – 5188.

[18] The average torsion value has been calculated from the torsion-angles values of the possible phenanthrenes subunits in the [5]-helicene, which has been obtained directly from the crystallographic data reported in R. J. Kuroda, *J. Chem. Soc. Perkin Trans. 2* **1982**, 789 – 794.

[19] J. Lu, D. M. Ho, N. J. Vogelaar, C. M. Kraml, R. A. Pascal, Jr., *J. Am. Chem. Soc.* **2004**, *126*, 11168 – 11169.

[20] D. G. Evans, J. C. A. Boeyens, *Acta Crystallogr. Sect. B* **1990**, *46*, 524 – 532.

[21] A.-C. Bédard, A. Vlassova, A. C. Hernandez-Perez, A. Bessette, G. Shanan, M. A. Heuft, S. K. Collins, *Chem. Eur. J.* **2013**, *19*, 16295 – 16302.

[22] Estimated from HOMO = $-5.10-E_{ox}$ (eV). See: C. M. Cardona, W. Li, A. E. Kaifer, D. Stockdale, G. C. Bazan, *Adv. Mater.* **2011**, *23*, 2367 – 2371.

[23] It has been demonstrated that when a carbonyl group is forced out of the plane, as is the case of **1** and **3**, leads to an increased fluorescence quenching, see: R. S. Anderson, N. V. Nagirimadugu, C. J. Abelt, *ACS Omega* **2019**, *4*, 14067 – 14073.

[24] Herein we focus on the structural features of a new family of chiral distorted HBCs analogues including a nonagon carbocycle. Detailed analysis of the excited state characteristics and kinetics of this new curved PAH backbone is ongoing although beyond the scope of this paper.

[25] H. Kubo, T. Hirose, T. Nakashima, T. Kawai, J.-Y. Hasegawa, K. Matsuda, *J. Phys. Chem. Lett.* **2021**, *12*, 686 – 695.

Manuscript received: July 13, 2021
Accepted manuscript online: July 30, 2021
Version of record online: August 24, 2021

